Pion-induced η production in the deuteron

H. Garcilazo[1] and M. T. Peña[2,3]
[1]*Escuela Superior de Física y Matemáticas, Instituto Politécnico Nacional, Edificio 9, 07738 México Distrito Federal, Mexico*
[2]*Centro de Física Nuclear da Universidade de Lisboa, P-1699 Lisboa Codex, Portugal*
[3]*Departamento de Física, Instituto Superior Técnico, P-1096 Lisboa Codex, Portugal*
(Received 30 November 1998)

We calculate the total cross section as well as single and double differential cross sections of the reaction $\pi^- d \to \eta nn$ for incident pion kinetic energies between threshold and 1500 MeV. Our model is based in a fully covariant formalism which includes the dominant single-scattering diagram as well as the nucleon-nucleon final-state interaction diagram. [S0556-2813(99)03905-9]

PACS number(s): 25.80.Hp, 14.40.Aq, 25.40.Ve

I. INTRODUCTION

Pion-induced production of η mesons in nuclei may proceed dominantly by the one-nucleon mechanism of the basic reactions $\pi^- p \to \eta n$ and $\pi^+ n \to \eta p$ [1,2]. In the two-nucleon system one can have the η produced in the deuteron by means of the reactions $\pi^- d \to \eta nn$ and $\pi^+ d \to \eta pp$ [3–5]. A closely related process is that of η production in nucleon-nucleon collisions such as $pp \to \eta pp$ [6], $pn \to \eta pn$, or $pn \to \eta d$ [7]. In this paper we are going to study the pion-induced η-production process in the deuteron in the energy region between threshold and 1500 MeV incident pion kinetic energy in order to see what are the dominant features of the cross section in this energy region and to compare with some available data at low energy.

The reactions $\pi^- d \to \pi^0 nn$ and $\pi^- d \to \eta nn$ look very similar in many respects. In fact, in the last reaction, one has simply replaced the π^0 by a heavier neutral meson. Thus, from the well-known features of the cross section for the pionic charge-exchange reaction in the deuteron one can already foresee much of what is to be expected for the behavior of the η-production cross section. The pionic charge-exchange reaction in the deuteron has been studied before extensively [8–10]. From these studies one knows first, that the Pauli principle plays a very important role and second, that the reaction is dominated by the single-scattering diagram. Therefore, these two ingredients should be also the starting point for a theoretical description of the η-production reaction. The next correction based on the previous experience with the pionic charge-exchange reaction is expected to be the nucleon-nucleon final-state interaction due to the strong $^1S_0$ NN interaction in the vicinity of zero relative energy. Thus, our model of pion-induced η production in the deuteron will consist of the four diagrams shown in Fig. 1. The processes 1(a) and 1(b) are, respectively, the single-scattering diagram and the final-state-interaction diagram while the processes 1(c) and 1(d) are their corresponding exchange diagrams.

One interesting aspect of the $\pi^- d \to \eta nn$ reaction is that due to the large mass difference between the initial and final mesons the exchanged nucleon in the dominant diagram 1(a) has the possibility to go much further off-the-mass-shell than in the pionic charge-exchange reaction where the initial and final mesons have the same mass. Thus, there is the hope that the η-production reaction may be more sensitive to those aspects of the system that depend on the off-shellness of this particle, such as the negative-energy components of the deuteron wave function [11,12], or the off-shell behavior of the elementary $\pi N \to \eta N$ amplitude. Moreover, given the order of magnitude of the momentum transfers involved in η-production processes, one has to invest effort in introducing relativistic effects in the nucleon-nucleon and η-nucleon dynamics. They may be needed at the short-range region of the interactions proved by these reactions. Therefore, the motivation to use a relativistic approach for the description of η production in nuclei is well accounted for. In this work we present the results of a calculation done within a relativistic approach.

Experimental data on the reactions $\pi N \to \pi N$ and $\pi N \to \eta N$ has already been obtained and analyzed, providing us with the knowledge of their associated transition matrices [1,2]. Since now also preliminary data for η production from πd scattering is already available [3–5], the possibility is there for modeling and testing the off-mass-shell extrapolation of the $\pi N \to \pi N$ and $\pi N \to \eta N$ amplitudes, which define their behavior in the nuclear medium. Calculations exist [13] already that include them in a coupled-channel

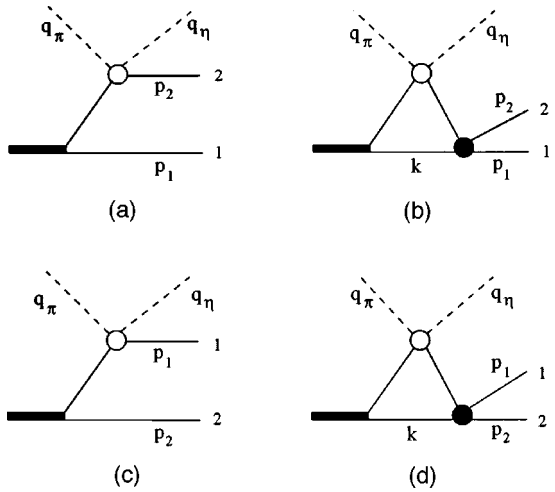

FIG. 1. Model of the reaction $\pi^- d \to \eta nn$: (a) single-scattering diagram, (b) final-state interaction diagram, (c) exchange diagrams of (a), and (d) exchange diagrams of (b).

study of the reactions of pion single charge-exchange ^{3}He$(\pi^-,\pi^0)^3$H and pion photoproduction ^{3}He$(\gamma,\pi^+)^3$H, at large momentum transfers. The results of this work show that the description used is not totally adequate for incident pion energies larger that 200 MeV, where it underestimates the data. The importance of trying to establish the off-mass-shell behavior of the $\eta N\to\eta N$ and $\pi N\to\eta N$ amplitudes is one of the main messages of Ref. [13], that also stresses that results for the pion-induced η production ^{3}He$(\pi^+,\eta)^3$H for energies below the free production threshold, underestimate the data, although for energies higher than 560 MeV the problems only exist for backward directions with large momentum transfer. The production of η's by pions is a relatively new field [3,4,13] that promises to be useful to gain insight in the meson-nuclear interaction. It is then clear that η production is stimulating experimental and theoretical work.

From the technical point of view, the $\pi N\to\eta N$ amplitude is not calculated from a coupled-channel set of covariant integral equations. However, the couplings for the meson-baryon-baryon vertices are taken to be modified effectively by energy-dependent functions phenomenologically adjusted to the on-mass-shell (experimental) constraints—phase shifts and inelasticities (this follows Ref. [14] where the method is applied to $\pi N\to\pi N$) which automatically guarantees that two-body unitarity is satisfied. A similar representation of the $NN\to NN$ amplitude is proposed here in order to describe the nucleon-nucleon final-state interaction.

In Sec. II we establish the formalism. In Sec. III we show the results and we present our conclusions in Sec. IV.

II. FORMALISM

The model we are going to use is depicted in Fig. 1. It consists of the single-scattering or impulse diagram 1(a), of the final-state interaction diagram 1(b), and of the corresponding exchange diagrams 1(c) and 1(d).

A. The amplitude for the process $\pi^- d\to\eta nn$

Labeling each partial amplitude that contributes to the process $\pi^- d\to\eta nn$ by the same letter that labels the corresponding diagram depicted in Fig. 1, the total amplitude is given by

$$A=A_a+A_b-A_c-A_d, \tag{1}$$

where the minus sign in the last two terms is required by the Pauli principle due to the two identical particles in the final state. The Feynman amplitude of the single-scattering process 1(a) is given by

$$A_a=\bar{u}_2(\vec{p}_2)t_{\pi N\to\eta N}\frac{\not K-\not q_\pi-\not p_1+M}{(K-q_\pi-p_1)^2-M^2+i\epsilon}V_{dNN}v_1(\vec{p}_1), \tag{2}$$

where K is the total four momentum, V_{dNN} is the deuteron-nucleon-nucleon vertex, $t_{\pi N\to\eta N}$ is the elementary η-production amplitude, and $v_1=i\gamma_2 u_1^*$ is a charge conjugate spinor for nucleon 1. The amplitude A_b of the final-state-interaction process 1(b) is given by

$$A_b=\frac{1}{(2\pi)^4}\int d^4k\bar{u}_2(\vec{p}_2)t_{NN\to NN}v_1(\vec{p}_1)\times i\frac{\not K-\not q_\eta-\not k+M}{(K-q_\eta-k)^2-M^2+i\epsilon}t_{\pi N\to\eta N}\times i\frac{\not K-\not q_\pi-\not k+M}{(K-q_\pi-k)^2-M^2+i\epsilon}V_{dNN}i\frac{\not k+M}{k^2-M^2+i\epsilon}, \tag{3}$$

with $t_{NN\to NN}$ being the amplitude for nucleon-nucleon scattering. We will evaluate the amplitude A_b by applying the spectator-on-mass-shell approximation [15]. That is, we integrate over the fourth component of the momentum k in Eq. (3) by closing the contour from below and assuming that only the pole at $k_0=\sqrt{M^2+\vec{k}^2}-i\epsilon\equiv E_k-i\epsilon$ contributes to the integral so as to get

$$A_b=\frac{1}{(2\pi)^3}\int\frac{M}{E_k}d\vec{k}\bar{u}_2(\vec{p}_2)\bar{v}_1(\vec{k})t_{NN\to NN}v_1(\vec{p}_1)\times\frac{\not K-\not q_\eta-\not k+M}{(K-q_\eta-k)^2-M^2+i\epsilon}t_{\pi N\to\eta N}\times\frac{\not K-\not q_\pi-\not k+M}{(K-q_\pi-k)^2-M^2+i\epsilon}V_{dNN}v_1(\vec{k}). \tag{4}$$

The amplitudes for the exchange diagrams 1(c) and 1(d) are obtained from Eqs. (2) and (4), respectively, by exchanging the coordinates and spins of particles 1 and 2. As a consequence of the spectator-on-mass-shell approximation, the spectator nucleon in the loop of Fig. 1(b) is put on the mass shell so that the deuteron-nucleon-nucleon vertex V_{dNN} and the nucleon-nucleon amplitude $t_{NN\to NN}$ are needed with only one nucleon off the mass shell. Similarly, in Fig. 1(a) the deuteron-nucleon-nucleon vertex has only one nucleon off the mass shell.

We carried out numerically the three-dimensional integration that appears in Eq. (4). The technical difficulty that arises relates to the process of handling the three-body singularities which appear when the exchanged nucleon in the rescattering process becomes on-mass shell. These singularities, however, were accurately integrated through an appropriate design of the integration mesh.

B. The dNN vertex

The deuteron-nucleon-nucleon vertex with one nucleon off the mass shell has the form [11,12]

$$V_{dNN}=F(k'^2)\not\epsilon_d+\frac{1}{M}G(k'^2)\epsilon_d\cdot k+\frac{\not k'-M}{M}\times\left[H(k'^2)\not\epsilon_d+\frac{1}{M}I(k'^2)\epsilon_d\cdot k\right], \tag{5}$$

where ϵ_d is the polarization vector of the deuteron and k and k' are the four momenta of the on-shell and off-shell nucleons, respectively. The form factors F, G, H, and I, are related to the four components of the deuteron wave function u, w, v_t, and v_s, where u and w are the usual upper components

described by the $^3S_1$ and $^3D_1$ states and v_t and v_s are the lower components described by the $^3P_1$ and $^1P_1$ states. As established by Gross and collaborators [11,12], the connection between the form factors and the four components of the deuteron wave function is

$$F(k'^2)=\pi\sqrt{2M_d}(2E-M_d)\left[u(p)-\frac{1}{\sqrt{2}}w(p)+\frac{M}{p}\sqrt{\frac{3}{2}}v_t(p)\right], \tag{6}$$

$$G(k'^2)=\pi\sqrt{2M_d}(2E-M_d)\left[\frac{M}{E+M}u(p)+\frac{M(2E+M)}{\sqrt{2}p^2}w(p)+\frac{M}{p}\sqrt{\frac{3}{2}}v_t(p)\right], \tag{7}$$

$$H(k'^2)=\pi\sqrt{2M_d}\,\frac{EM}{p}\sqrt{\frac{3}{2}}v_t(p), \tag{8}$$

$$I(k'^2)=-\pi\sqrt{2M_d}\,\frac{M^2}{M_d}\left\{(2E-M_d)\left[\frac{1}{E+M}u(p)-\frac{E+2M}{\sqrt{2}p^2}w(p)\right]+\frac{M_d}{p}\sqrt{3}v_s(p)\right\}, \tag{9}$$

where M_d is the mass of the deuteron, $E=\sqrt{p^2+M^2}$, and p is the magnitude of the nucleon-nucleon relative three-momentum in the c.m. frame which is a Lorentz invariant given by

$$p^2=\frac{(M_d^2+M^2-k'^2)^2}{4M_d^2}-M^2. \tag{10}$$

The wave functions of the deuteron u, w, v_t, and v_s, have been constructed by Buck and Gross [11] by considering six different one-boson-exchange models for the NN interaction. Those models were fitted to reproduce the static properties of the deuteron. For the πNN vertex those models consider a linear combination of pseudovector and pseudoscalar coupling as

$$\Gamma_{\pi NN}=\lambda\gamma_5+(1-\lambda)\frac{1}{2M}\gamma_5\not{q}_\pi, \tag{11}$$

where the running value λ varies from $\lambda=0$ (corresponding to pure pseudovector coupling) to $\lambda=1$ (corresponding to pure pseudoscalar coupling).

C. The $\pi N\to\eta N$ amplitude

We will use for the $\pi N\to\eta N$ scattering amplitude a variable-mass isobar model [14,15] which is depicted in Fig. 2(a). The spin-$\frac{1}{2}$ and spin-$\frac{3}{2}$ isobars have a mass equal to the invariant mass of the system $\sqrt{s}$ and the meson-nucleon-isobar couplings are chosen such as to generate scattering in the orbital angular momenta $l_\pm=j\pm\frac{1}{2}$. The explicit form of the amplitude is

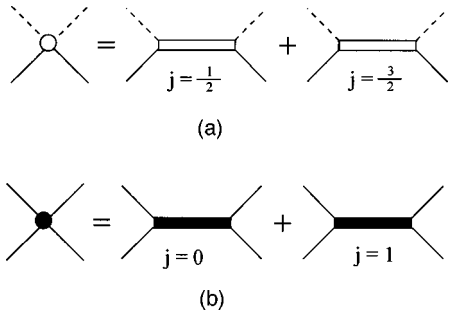

FIG. 2. Isobar model of the (a) $\pi N\to\eta N$ and (b) $NN\to NN$ amplitudes.

$$t_{\pi N\to\eta N}=f_0^{1/2}(s)(\not{P}+\sqrt{s})+f_1^{1/2}(s)(\not{P}-\sqrt{s})+f_1^{3/2}(s)(\not{P}+\sqrt{s})\left[-q\cdot q'+\frac{\not{q}\not{q}'}{3}+\frac{2P\cdot qP\cdot q'}{3s}-\frac{P\cdot q\not{q}'-\not{q}P\cdot q'}{3\sqrt{s}}\right]+f_2^{3/2}(s)(\not{P}-\sqrt{s})\left[-q\cdot q'+\frac{\not{q}\not{q}'}{3}+\frac{2P\cdot qP\cdot q'}{3s}+\frac{P\cdot q\not{q}'-\not{q}P\cdot q'}{3\sqrt{s}}\right], \tag{12}$$

where $s=P^2=(q_\eta+p_2)^2$ in the notation of Fig. 1(a). The transition amplitude for the specific charge states that are needed in this work are

$$t_{\pi^+n\to\eta p}=\sqrt{2/3}t_{\pi N\to\eta N}, \tag{13}$$

$$t_{\pi^-p\to\eta n}=-\sqrt{2/3}t_{\pi N\to\eta N}. \tag{14}$$

If one evaluates $\bar{u}_2(\vec{p}_2)t_{\pi N\to\eta N}u_2(\vec{p}_2')$ in the two-body c.m. frame, the first two terms in Eq. (12) generate the scattering amplitude with $j=1/2$ for $l=0$ and $l=1$, respectively, while the last two terms generate the scattering amplitude with $j=3/2$ for $l=1$ and $l=2$, respectively. Therefore, the functions $f_l^j(s)$ are directly related to the corresponding partial-wave transition amplitudes $\tau_l^j(s)$ normalized as in the Argand diagram by

$$f_0^{1/2}(s)=-\frac{4\pi}{\sqrt{(E+M)(E'+M)}}\frac{1}{\sqrt{pp'}}\tau_0^{1/2}(s), \tag{15}$$

$$f_1^{1/2}(s)=-4\pi\sqrt{(E+M)(E'+M)}\frac{1}{pp'\sqrt{pp'}}\tau_1^{1/2}(s), \tag{16}$$

$$f_1^{3/2}(s)=-\frac{12\pi}{\sqrt{(E+M)(E'+M)}}\frac{1}{pp'\sqrt{pp'}}\tau_1^{3/2}(s), \tag{17}$$

$$f_2^{3/2}(s)=-12\pi\sqrt{(E+M)(E'+M)}\frac{1}{p^2p'^2\sqrt{pp'}}\tau_2^{3/2}(s), \tag{18}$$

where

$$E=\sqrt{p^2+M^2}, \tag{19}$$

$$E'=\sqrt{p'^2+M^2}, \tag{20}$$

$$p^2=\frac{1}{4s}[s-(M+m)^2][s-(M-m)^2], \tag{21}$$

$$p'^2=\frac{1}{4s}[s-(M+m')^2][s-(M-m')^2], \tag{22}$$

with m and m' being the masses of the initial and final mesons, respectively. The $\pi N\to\eta N$ partial-wave transition amplitudes $\tau_l^j(s)$ that appear in Eqs. (15)–(18) have been obtained recently by Batinić *et al.* [1,2] by fitting all the available data on the reactions $\pi N\to\pi N$ and $\pi N\to\eta N$ [16].

Equation (12) is valid when any of the four particles in the $\pi N\to\eta N$ amplitude is off-mass-shell. For example, in all the diagrams of Fig. 1 the two mesons are on-mass shell while in diagrams 1(a) and 1(c) one of the nucleons is off-mass shell and in diagrams 1(b) and 1(d) the two nucleons are off-mass shell. Therefore, it is interesting to explore the off-shell behavior of the $\pi N\to\eta N$ amplitude given by Eq. (12) by introducing form factors that are equal to one if the nucleons are on-mass shell and less than one when the nucleons become off-mass shell. Thus, we will generalize Eq. (12) as

$$t_{\pi N\to\eta N}\to e^{(p_2^2-M^2)/\Lambda^2}t_{\pi N\to\eta N}e^{(p_1^2-M^2)/\Lambda^2}, \tag{23}$$

where p_1 and p_2 are the momenta of the initial and final nucleons and Λ is a free parameter.

D. The $NN\to NN$ amplitude

The final-state-interaction diagram 1(b) contains the nucleon-nucleon scattering amplitude $t_{NN\to NN}$ which becomes large when the two neutrons have relative energy close to zero due to the presence of a virtual bound state in the $^1S_0$ channel. We will model the $NN\to NN$ amplitude in a way similar to that of the $\pi N\to\eta N$ system which is depicted in Fig. 2(b). We note that the calculation of the production amplitudes demand the knowledge of the NN interaction when one of the nucleons is off-its-mass shell, which therefore prevents its description through a traditional nonrelativistic potential. We will consider then spin-0 and spin-1 isobars and the nucleon-nucleon-isobar couplings will be chosen such that they generate scattering in the orbital angular momentum states $l=0$ and $l=1$, i.e., in the $^1S_0$, $^3P_0$, and $^3P_1$ channels. In our model the off-mass-shell behavior will be determined by the Lorentz structure of propagators and couplings. The vertices will be dressed as a result of implementing unitarity, through the solution of the integral scattering equation. The advantage of this formulation lies in providing directly the Lorentz structure for the NN scattering transition matrix suitable to be included in the amplitudes of the production diagrams, and which is the analogue for the scattering case of the deuteron vertex in the form of Eq. (5).

The $NN\to NN$ amplitude with one of the initial nucleons off the mass shell will then be taken as

$$\bar{u}_2(\vec{p}_2)\bar{v}_1(\vec{k})t_{NN\to NN}v_1(\vec{p}_1)=\bar{u}_2(\vec{p}_2)\gamma_5 v_1(\vec{p}_1)f_{00}^0(s;k'^2)\bar{v}_1(\vec{k})\gamma_5+\bar{u}_2(\vec{p}_2)v_1(\vec{p}_1)f_{11}^0(s;k'^2)\bar{v}_1(\vec{k})$$
$$+\bar{u}_2(\vec{p}_2)\gamma^\mu\gamma_5 v_1(\vec{p}_1)f_{11}^1(s;k'^2)\left(-g_{\mu\nu}+\frac{P_\mu P_\nu}{s}\right)\bar{v}_1(\vec{k})\gamma^\nu\gamma_5, \tag{24}$$

where

$$k'=p_1+p_2-k, \tag{25}$$

is the four-momentum of the off-shell nucleon,

$$P=k+k'=p_1+p_2, \tag{26}$$

is the total four-momentum of the NN subsystem, while

$$s=P^2, \tag{27}$$

is the invariant mass squared of the NN subsystem. The functions $f_{ls}^j(s;k'^2)$ are directly related to the corresponding partial-wave elastic amplitudes $t_{ls}^j(p,p_0;s)$ by

$$f_{00}^0(s;k'^2)=-\frac{4\pi}{\sqrt{s}p_0}t_{00}^0(p,p_0;s), \tag{28}$$

$$f_{11}^0(s;k'^2)=-\frac{\pi\sqrt{s}}{p_0^3}\frac{p_0}{p}t_{11}^0(p,p_0;s), \tag{29}$$

$$f_{11}^1(s;k'^2)=-\frac{3}{2}\frac{\pi\sqrt{s}}{p_0^3}\frac{p_0}{p}t_{11}^1(p,p_0;s), \tag{30}$$

where $t_{ls}^j(p,p_0;s)$ is the half-energy-shell T matrix normalized such that

$$t_{ls}^j(p_0,p_0;s)=\sin\delta_{ls}^j(s)e^{i\delta_{ls}^j(s)}, \tag{31}$$

and p is the magnitude of the nucleon-nucleon relative three-momentum in the c.m. frame which is a Lorentz invariant given by

$$p^2=\frac{[s+M^2-k'^2]^2}{4s}-M^2, \tag{32}$$

while p_0 is the corresponding on-shell momentum which is obtained by setting $k'^2=M^2$ in Eq. (32), i.e.,

$$p_0^2=\frac{s}{4}-M^2. \tag{33}$$

For the half-energy-shell T matrices that appear in Eqs. (28)–(30) we used the solutions obtained using the Paris potential [17] in the Blankenbecler-Sugar equation. The relativistic Blankenbecler-Sugar equation is related to the nonrelativistic Lippmann-Schwinger equation by means of the minimal relativity transformation [18].

E. The cross section

Since in the measurements that are being performed [3,4] only the η meson is detected, one has to calculate the inclusive differential cross section. Therefore, it is more convenient to calculate the cross section in the three-body c.m. system and then transform it to the laboratory system. The kinematically complete differential cross section in the three-body frame is given by

$$\frac{d^3\sigma}{d\Omega_\eta dq_\eta d\Omega_N} = \frac{M^2 q_\eta^2 p_N}{48(2\pi)^5 \sqrt{S} q_\pi \omega_\eta \sqrt{s}} \sum_{\text{spins}} |A|^2, \quad (34)$$

where q_π, q_η, and p_N are, respectively, the magnitudes of the three momenta of the initial pion, final η, and relative nucleon-nucleon, $\sqrt{S}$ and $\sqrt{s}$ are the invariant masses of the three-body system and nucleon-nucleon subsystem, respectively, while

$$\omega_\eta = \sqrt{m_\eta^2 + q_\eta^2}, \quad (35)$$

$$s = (\sqrt{S} - \omega_\eta)^2 - q_\eta^2, \quad (36)$$

$$p_N = \sqrt{s/4 - M^2}. \quad (37)$$

The inclusive differential cross section is given by

$$\frac{d^2\sigma}{d\Omega_\eta dq_\eta} = \int d\Omega_N \frac{d^3\sigma}{d\Omega_\eta dq_\eta d\Omega_N}. \quad (38)$$

Finally, the inclusive differential cross section in the laboratory system is obtained as

$$\frac{d^2\sigma}{d\Omega dq} = \frac{d^2\sigma}{d\Omega_\eta dq_\eta} \frac{q^2 \sqrt{q_\eta^2 + m_\eta^2}}{q_\eta^2 \sqrt{q^2 + m_\eta^2}}, \quad (39)$$

where q is the magnitude of the three momentum of the η in the laboratory frame. The single differential cross section is given by

$$\frac{d\sigma}{d\Omega} = \int dq \frac{d^2\sigma}{d\Omega dq}, \quad (40)$$

while the integrated total cross section is

$$\sigma = \int d\Omega \frac{d\sigma}{d\Omega}. \quad (41)$$

III. RESULTS

We will now use the formalism of the previous section to investigate the main features of the cross section for the $\pi^- d \to \eta nn$ process. For all the calculations that follow except when otherwise stated we will use $\lambda = 0$ in Eq. (11) which corresponds to having pure pseudovector coupling in the πNN vertex of the deuteron wave function [11]. Similarly, we will take $\Lambda = \infty$ in Eq. (23) which corresponds to no form factors at all when the nucleons become off-mass shell in the $\pi N \to \eta N$ amplitude. At the end we will examine the sensitivity of the results to the off-shell effects originating from these two sources. Also, unless otherwise stated, all the angles, energies, and momenta refer to the laboratory system.

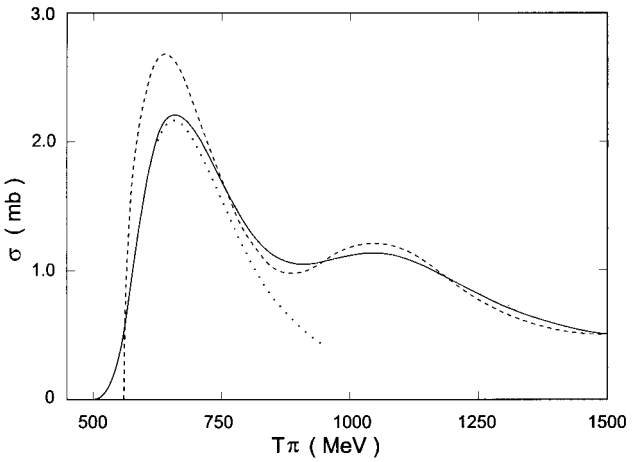

FIG. 3. Total cross section of the reaction $\pi^- d \to \eta nn$ as a function of incident pion kinetic energy (solid line). Also shown is the total cross section of the reaction $\pi^- p \to \eta n$ (dashed line) and the total cross section of the reaction $\pi^- d \to \eta nn$ calculated considering only the S_{11} channel in the $\pi N \to \eta N$ amplitude (dotted line).

We show in Fig. 3 the integrated total cross section of the $\pi^- d \to \eta nn$ process between threshold and 1500 MeV incident pion kinetic energy (solid line). We also show for comparison the total $\pi^- p \to \eta n$ cross section calculated using Eq. (12) and the amplitudes of [1,2,16] (dashed line). The first thing that can be noticed is that the two cross sections are similar. This is just a reflection of the fact that the single-scattering diagram 1(a) is the dominant process of η production in the deuteron. The largest difference between the $\pi^- d \to \eta nn$ and $\pi^- p \to \eta n$ cross sections is at the position of the first peak where the cross section in the deuteron is about 20% lower than the cross section in the proton. The threshold for η production from the proton is 560 MeV and the threshold for η production from the deuteron is 488 MeV. Notice, however, that while at threshold the cross section for η production from the proton rises very sharply, the cross section for η production from the deuteron rises quite softly which is a consequence of the Fermi motion of the proton inside the deuteron. We have also drawn with dotted lines the total $\pi^- d \to \eta nn$ cross section calculated including only the contribution of the S_{11} channel in the $\pi N \to \eta N$ transition amplitude [the first term in the right-hand side of Eq. (12)]. Both curves are very close for energies up to about 650 MeV. This shows that the S_{11} resonance dominates the process for energies below 650 MeV. The effect of the nucleon-nucleon final-state interaction is to lower the $\pi^- d \to \eta nn$ cross section by about 2% at the position of the first peak and to raise it by a similar amount at higher energies. Probably, very close to threshold the contribution of the double-scattering term which involves the $\eta N \to \eta N$ amplitude is important. However, since there is no direct data for

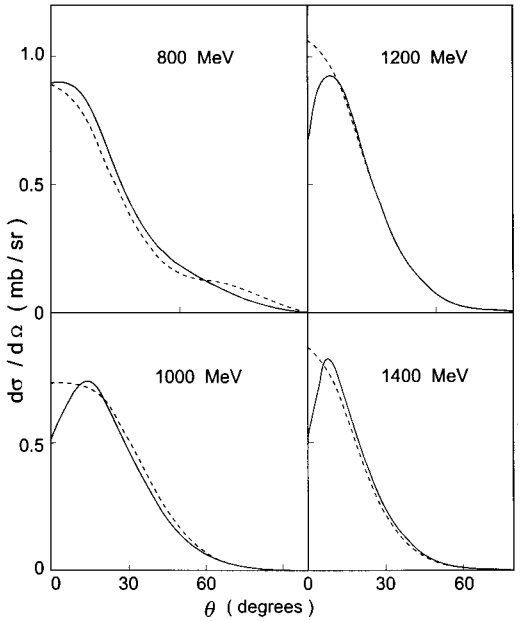

FIG. 4. Differential cross section in the laboratory system for the reaction $\pi^- d \to \eta nn$ at four incident pion kinetic energies (solid lines). The dashed lines are the differential cross sections from a free proton.

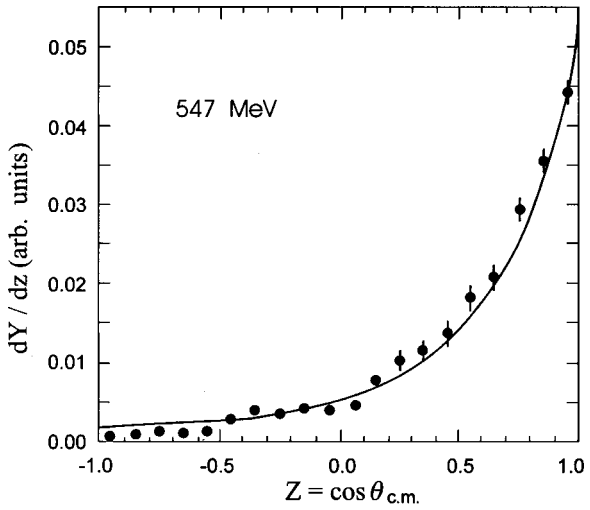

FIG. 5. Differential yield in the c.m. system for the reaction $\pi^- d \to \eta nn$ at 547 MeV (670 MeV/c) incident pion kinetic energy. The data are from [3,4].

the $\eta N \to \eta N$ process the calculation of that contribution would be less reliable than the ones presented here.

We show in Fig. 4 the predictions of our model for the differential cross section $d\sigma/d\Omega$ at four different energies. For comparison, we show with dashed lines the corresponding cross sections for η production from the proton. The most outstanding feature that can be observed in this figure is that for energies larger that ~800 MeV there is a suppression of the differential cross section at small angles. This behavior is caused by the Pauli principle that is acting in the $\pi^- d \to \eta nn$ reaction since there one has two identical particles in the final state. This so-called Pauli suppression is a very important effect in the $\pi^- d \to \pi^0 nn$ reaction where the reduction at small angles amounts approximately to a factor of 20 and it shows up for all energies [8–10]. In the case of the $\pi^- d \to \eta nn$ process, there is a mismatch between the initial and final momenta of the mesons due to the mass difference between them. This has the consequences that here the Pauli suppression is much weaker and moreover it appears only for energies above 800 MeV.

Comparison with some preliminary data for the yield [3,4] at 547 MeV ($q_{\rm LAB}=670$ MeV/c) is shown in Fig. 5. In this case we have normalized the theoretical curve to the largest data point since the data is given in arbitrary units. As one can see the agreement with the data is quite good.

We show in Fig. 6 the double differential cross section $d^2\sigma/d\Omega dq$ at 700 MeV for five different angles of the outgoing η. We also show with dashed lines the results without the effect of the final-state-interaction (FSI) diagram. As it can be seen from this figure, the influence of the nucleon-nucleon FSI is at most a few percent. The FSI in the $NN\ ^1S_0$ channel is strong only when the relative energy of the two neutrons is close to zero which corresponds to the upper end of the η momentum. However, the region where the cross section is large (the quasielastic peak) does not coincide with the upper end of the spectrum so that the cross section is very small when the FSI is large. Another reason for the weakness of the FSI in the $\pi^- d \to \eta nn$ process is the fact that if the two neutrons are in the $^1S_0$ channel then one is going from an initial πd state to a final $\eta d'$ state where d' is a nucleon-nucleon isobar with spin 0. Therefore, by parity conservation, the transition from an initial state where the deuteron has helicity zero is forbidden. Thus, out of the three possible initial helicities only two of them are allowed which means that for the $^1S_0$ channel one has roughly only 2/3 of the FSI contributing to the process.

We now come to the question of how sensitive is the $\pi^- d \to \eta nn$ reaction to off-shell effects. First, we have studied the sensitivity of the $\pi^- d \to \eta nn$ process to the negative-energy components of the deuteron wave function [v_s and v_t components in Eqs. (6)–(9)] by considering the six models of Buck and Gross [11] which have different admixtures probabilities of negative-energy components. In the previous

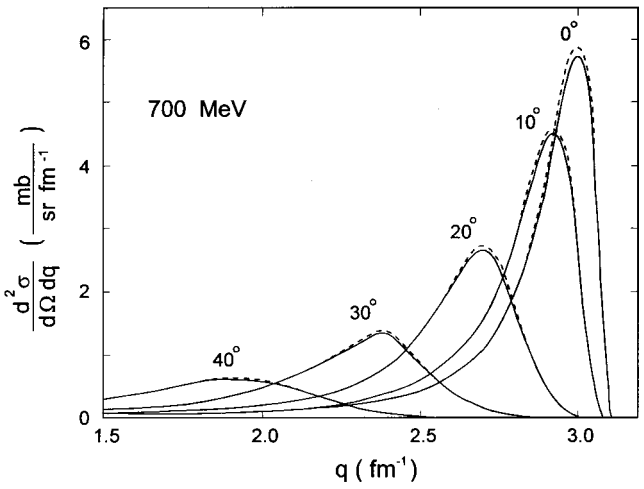

FIG. 6. Double differential cross section in the laboratory system for the reaction $\pi^- d \to \eta nn$ at five different angles of the outgoing η for an incident pion kinetic energy of 700 MeV.

results we have always used $\lambda=0$ in Eq. (11) which corresponds to having pure pseudovector coupling in the model that generates the deuteron wave function. For that case, the probability of the negative-energy components is very small. If λ is increased the probability of the negative-energy components also increases being maximum when $\lambda=1$. We show in Fig. 7 the differential cross section at 600 and 1300 MeV with our standard model that uses $\lambda=0$ (solid line) and with the model that uses $\lambda=1$ (dashed line). The effect on the differential cross section at 1300 MeV is an increase of less than 10% and a somewhat smaller increase at 600 MeV. Second, we studied the effect of introducing form factors in the $\pi N\rightarrow\eta N$ amplitude when the nucleons go off-mass shell [see Eq. (23)]. We show in Fig. 7 with dotted lines the results that are obtained when we use $\lambda=0$ and put $\Lambda=1000$ MeV/c in Eq. (23). In this case the effect on the differential cross section is the opposite and we obtain reductions of comparable magnitudes.

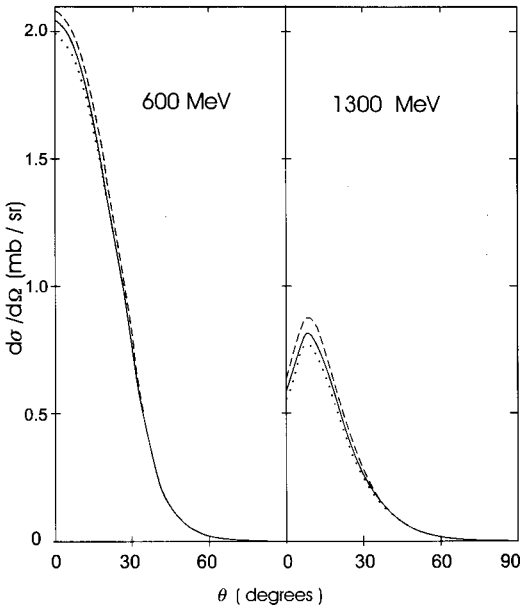

FIG. 7. Differential cross section in the laboratory system for the reaction $\pi^-d\rightarrow\eta nn$ at two incident pion kinetic energies. The solid lines are the results obtained with $\lambda=0$ and $\Lambda=\infty$ in Eqs. (11) and (23), respectively. The dashed lines are the results obtained with $\lambda=1$ and $\Lambda=\infty$ and the dotted lines are the results obtained with $\lambda=0$ and $\Lambda=1000$ MeV/c.

IV. CONCLUSIONS

We have studied the main features of the cross section of the $\pi^-d\rightarrow\eta nn$ process. By comparing with the η-production cross section on a free proton we have isolated the effects of Fermi motion, the Pauli principle, the nucleon-nucleon FSI, and the dependence on off-shell effects. As for comparison with experimental data, we succeed in describing the one which exists at the moment. More data would be welcome.

ACKNOWLEDGMENTS

We thank Dr. A. Švarc for very valuable communications and comments on the subject of this paper. This work was supported in part by COFAA-IPN (Mexico) and by Fundação para a Ciência e a Tecnologia, MCT, under Contracts No. PRAXIS XXI/BCC/18975/98 and No. PRAXIS/P/FIS/10031/1998 (Portugal).

[1] M. Batinić, I. Šlaus, A. Švarc, and B. M. K. Nefkens, Phys. Rev. C **51**, 2310 (1995).
[2] M. Batinić, I. Dadić, I. Šlaus, A. Švarc, B. M. K. Nefkens, and T.-S. H. Lee, Phys. Scr. **58**, 15 (1998).
[3] R. Chrien (private communication).
[4] A. Marušić, Ph.D. thesis, University of Sagreb, 1996.
[5] AGS at Brookhaven National Laboratory: Experiment E890.
[6] M. Batinić, A. Švarc, and T.-S. H. Lee, Phys. Scr. **56**, 321 (1997).
[7] H. Calén *et al.*, Phys. Rev. Lett. **80**, 2069 (1998).
[8] H. Garcilazo, Phys. Rev. Lett. **65**, 293 (1990).
[9] H. Garcilazo, Phys. Rev. C **47**, 957 (1993).
[10] H. Garcilazo, Phys. Rev. C **53**, R20 (1996).
[11] W. W. Buck and F. Gross, Phys. Rev. D **20**, 2361 (1979).
[12] R. G. Arnold, C. E. Carlson, and F. Gross, Phys. Rev. C **21**, 1426 (1980).
[13] S. S. Kamalov, L. Tiator, and C. Benhold, Phys. Rev. C **47**, 941 (1993).
[14] H. Garcilazo and E. Moya de Guerra, Phys. Rev. C **52**, 49 (1995).
[15] H. Garcilazo, Phys. Rev. C **35**, 1804 (1987).
[16] We thank Dr. A. Švarc for sending us the most recent solution in numerical form.
[17] M. Lacombe, B. Loiseau, J. M. Richard, R. Vinh Mau, J. Côté, P. Pirès, and R. de Tourreil, Phys. Rev. C **21**, 861 (1980).
[18] G. E. Brown and A. D. Jackson, *The Nucleon-Nucleon Interaction* (North-Holland, Amsterdam, 1976).